Influence of Mean Water Depth and a Subsurface Sandbar on the Onset and Strength of Wave Breaking

JIN-BAO SONG

Institute of Oceanology, Chinese Academy of Sciences, Qingdao, China

MICHAEL L. BANNER

School of Mathematics, The University of New South Wales, Sydney, New South Wales, Australia

(Manuscript received 5 July 2002, in final form 22 September 2003)

ABSTRACT

Wave breaking in the open ocean and coastal zones remains an intriguing yet incompletely understood process, with a strong observed association with wave groups. Recent numerical study of the evolution of fully nonlinear, two-dimensional deep water wave groups identified a robust threshold of a diagnostic growth-rate parameter that separated nonlinear wave groups that evolved to breaking from those that evolved with recurrence. This paper investigates whether these deep water wave-breaking results apply more generally, particularly in finite-water-depth conditions. For unforced nonlinear wave groups in intermediate water depths over a flat bottom, it was found that the upper bound of the diagnostic growth-rate threshold parameter established for deep water wave groups is also applicable in intermediate water depths, given by $k_0h \geq 2$, where k_0 is the mean carrier wavenumber and h is the mean depth. For breaking onset over an idealized circular arc sandbar located on an otherwise flat, intermediate-depth ($k_0h \geq 2$) environment, the deep water breaking diagnostic growth rate was found to be applicable provided that the height of the sandbar is less than one-quarter of the ambient mean water depth. Thus, for this range of intermediate-depth conditions, these two classes of bottom topography modify only marginally the diagnostic growth rate found for deep water waves. However, when intermediate-depth wave groups ($k_0h \geq 2$) shoal over a sandbar whose height exceeds one-half of the ambient water depth, the waves can steepen significantly without breaking. In such cases, the breaking threshold level and the maximum of the diagnostic growth rate increase systematically with the height of the sandbar. Also, the dimensions and position of the sandbar influenced the evolution and breaking threshold of wave groups. For sufficiently high sandbars, the effects of bottom topography can induce additional nonlinearity into the wave field geometry and associated dynamics that modifies the otherwise robust deep water breaking-threshold results.

1. Introduction

Breaking surface gravity waves play an important role in the exchange of energy, momentum, heat, gases, and water vapor between the atmosphere and the ocean, affecting the evolution of wind waves, the formation of surface currents, the distribution of near-surface turbulence both in the open ocean and in the coastal zone, as well as the marine meteorological conditions. Progress on various aspects of wave breaking over the past 25 yr is reviewed by a number of authors—for example, in the surf zone (Peregrine 1983), deep water breaking (Banner and Peregrine 1993), in air–sea interaction (Melville 1996; Thorpe 1995), and spilling breakers (Duncan 2001). Very recently, in the open-ocean context, there has been renewed scientific interest on routes to breaking in deep water, particularly on the underlying role of wave groups (Tulin and Waseda 1999), parameterizing breaking occurrence (Banner et al. 2002), and spectral breaking-wave statistics (Melville and Matusov 2002). The coastal-waves community has been more concerned with breaking criteria (e.g., breaker height index), induced currents and spectral transformation for shoaling breaking waves over flat reefs, sloping beaches, and sandbar topography (e.g., Nelson 1994; Beji and Battjes 1993; Svendsen and Veeramony 2001, among many others). It is evident that wave group influence has been a persistent but unresolved issue.

Motivated by the close association of nonlinear wave group behavior and deep water wave breaking, Song and Banner (2002, henceforth SB02) studied numerically the evolution to breaking or recurrence of fully nonlinear, two-dimensional inviscid wave groups in deep water. They identified a growth-rate parameter associated with the mean energy flux to the energy maximum in the wave group and found that it provides a

Corresponding author address: Prof. Michael L. Banner, School of Mathematics, The University of New South Wales, Sydney 2052, New South Wales, Australia.
E-mail: m.banner@unsw.edu.au

robust threshold indicator for recurrence or breaking onset behavior. This dynamically based approach provides an earlier and more decisive prediction of breaking onset than previously proposed breaking thresholds and potentially predicts the breaking strength. Also, Banner and Song (2002) found that the addition of wind forcing and/or a surface layer shear generally resulted in small departures from the results for the unforced cases reported in SB02, indicating that nonlinear energy fluxes within a wave group dominate the evolution to recurrence or breaking even in the presence of these other mechanisms.

When ocean waves interact with the bottom bathymetry, it is well-known that their dynamics can depart significantly from deep water behavior (e.g., Peregrine 1983). The unresolved large discrepancy between breaker height index on flat-topped and sloping coastal reef topography reported by Nelson (1994) is one example that highlights an incomplete fundamental understanding of breaking onset in finite water depths. A closely related phenomenon is the dynamics of waves shoaling over offshore sandbars in the coastal zone and the subsequent sandbar evolution. Such near-shore sandbars are found along several continental coasts. For example, the shoaling wave study of Elgar et al. (1997) at Duck, North Carolina, reported sandbar widths of around 100 m and heights of 1 m submerged about 1.5–2.5 m below the mean sea surface, with offshore significant wave heights of 0.4–2.7 m and frequencies from 0.05 to 0.25 Hz. On the Netherlands coast (about 120 km from Den Helder to Hoek Van Holland), Winjberg and Terwindt (1995) studied the evolution of sandbars 100–200 m wide and 2–3 m high, submerged about 2–4 m under the action of incident waves of mean height and period about 1.2 m and 5 s. Other studies with sandbar geometries relevant to the present study are described in Lippmann et al. (1993), Ruessink and Kroon (1994), Plant et al. (1999), Shand and Bailey (1999), and Kuriyama (2002).

In this context, the present study investigates wave breaking onset in nonlinear wave groups in the presence of generic bottom topographical features of interest in coastal oceanography. The deep water study of SB02 was extended to shallower water depths, focusing on the influence of finite uniform water depth and of a bottom sandbar on their proposed deep water breaking threshold.

2. Methodology

In brief, the present study utilized two fully nonlinear, two-dimensional wave codes: a periodic domain model developed by Dold and Peregine (1986, henceforth DP86) and a numerical wave tank model developed by Y. Agnon and N. Drimer (1998, personal communication), with refinements by A. Segre (1998, personal communication), henceforth referred to as the DAS code. Further details of these codes are given in section 2a of SB02. The evolution to breaking or recurrence of various classes of wave groups was investigated, with the essential features of two-dimensional wave breaking captured by each of these codes well into the overturning regime without numerical smoothing. A summary of the approach and methodology is given below, but the reader is referred to SB02 for a fuller description of the computational techniques and accuracy.

The present investigation addresses intermediate-depth water waves where the undisturbed water depth h is taken as 2, 3, or 4 units in conjunction with the initial (reference) carrier wavelength $\lambda = 2\pi$ units used throughout this study in order to make direct comparisons with our previous deep water results in SB02. The corresponding reference carrier wavenumber $k_0 = 1$ provides a consistent normalization for all length scales, so that their dimensional and nondimensional forms are identical. The intermediate-depth limitation was necessary because we found that the versions of the above codes that were available to us could not reliably simulate marginal breaking or recurrent shallow water waveforms for mean water depths $h < 2$.

Two numerical wave tank configurations were utilized in this study in conjunction with the DAS code. The first wave tank setup, shown in Fig. 1a, illustrates the case of a uniform flat bottom. Here, h is the undisturbed water depth near the piston and the parameters x_1 and x_2 control the slope of the downstream beach, for which we took $x_1 = 50\pi$ and $x_2 = x_1 + 20$ in our calculations. A second numerical wave tank configuration was used to investigate rapid forcing of nonlinear wave groups by bottom topography, here a submerged sandbar. A circular arc ''sandbar'' was formulated into the DAS code as part of the lower boundary (Γ_b) of the numerical wave channel, as shown in Fig. 1b. Here, x_0 is the x coordinate of the center of the bar, l_0 is its length, and h_0 is its height, and the parameters h, x_1, and x_2 have the same meaning as above. The points (x, y) on the circular arc profile satisfy

$$(x - x_0)^2 + (y - h_0 + h + R)^2 = R^2;$$

$$R = \frac{1}{2h_0}\left(\frac{1}{4}l_0^2 + h_0^2\right). \quad (1)$$

These parameters were varied in our calculations to explore the influence of sandbar and water-depth geometry on breaking onset, over a parameter space representative of observed sandbar conditions as described in the preceding section.

For each model domain (periodic or wave tank) investigated, wave groups with moderate initial carrier wave steepness were found to have two diverse modes of evolution—either pseudorecurrence to the original wave group structure, or evolution to breaking. Several classes of initial wave group structures were investigated in this study. The cases are named so that they can be compared with their deep water counterparts in

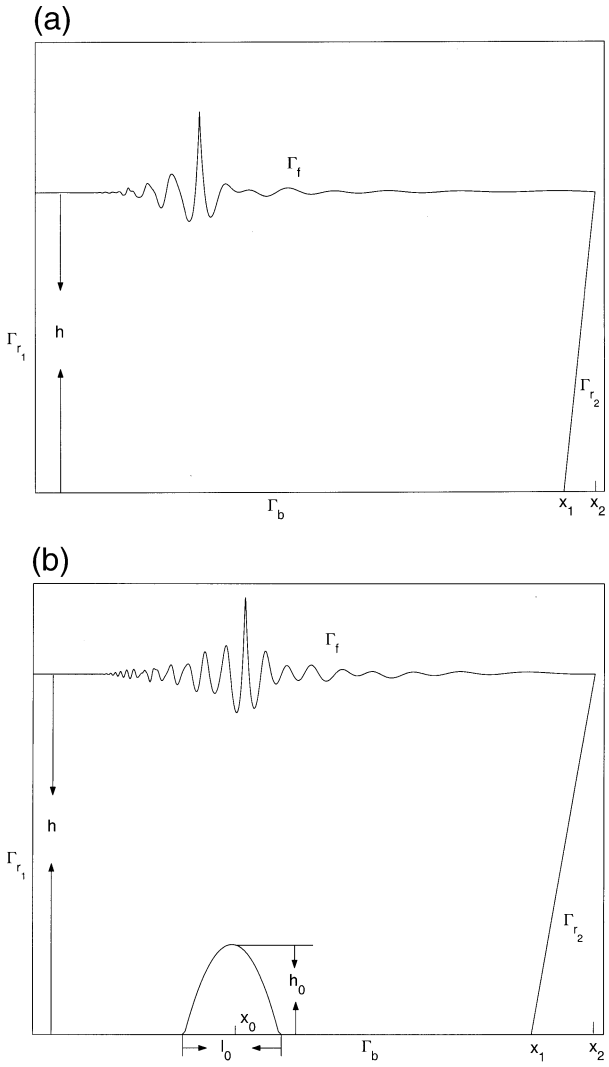

FIG. 1. (a) Typical numerical wave tank with a flat bottom: Γ_{r_1} is the piston end, Γ_f is the free surface, Γ_{r_2} is the absorbing beach, Γ_b is the bottom, and h is the undisturbed water depth. Note the strong vertical exaggeration. (b) Typical numerical wave tank configuration with a sandbar on an otherwise flat bottom: Γ_{r_1}, Γ_f, Γ_{r_2}, and Γ_b are the boundaries. The bottom sandbar has its center at x_0 with height h_0 and length l_0. Other details are as in (a).

SB02. Case I wave groups, propagating in a periodic domain, comprised a fundamental carrier wave with two small symmetric sidebands, using as parameters the initial carrier wave amplitude a_0 (or steepness $s_0 = a_0k_0$, where the center carrier wavenumber $k_0 = 1$) and the number of waves in one modulation length N, where $3 \leq N \leq 10$. Case III waves were a class of wave tank chirped wave packets in which the leading waves generated are overtaken by faster-moving longer waves generated subsequently by the paddle motion. For comparison, we also investigated two other wave group geometries designated, respectively, cases IV and V. Case IV wave groups were wave tank packets corresponding to case I periodic wave groups, while case V, with a much more rapid deformation than case III and case IV, emulated case II periodic domain waves with a bimodal initial spectrum studied in SB02. Mathematical details of the initial wave forms are given in the appendix, and typical evolving wave packets are shown graphically in Fig. 1 and also in SB02 in greater detail.

The analysis methodology of the present computational results is summarized as follows. The primary analysis consisted of calculating the surface wave profile and the associated subsurface velocity field at each time step, from which the total depth-averaged energy of the motion was computed as a horizontal distribution. After conversion to a quasi–wave-steepness distribution using the local energy density and smoothed local wavenumber of the surface elevation, its envelope maximum $\mu(t)$ was determined. Because of the asymmetry of the wave profile, $\mu(t)$ is oscillatory and its local average $\langle\mu(t)\rangle$ gives a measure of the mean convergence rate at the envelope maximum. From $\langle\mu(t)\rangle$, the intrinsic nondimensional growth rate $\delta(t) = D\langle\mu\rangle/\omega_0 Dt$ was computed, where ω_0 is the linear carrier wave frequency calculated from k_0 and D/Dt is the derivative traveling with the group energy maximum. The major finding from SB02 and Banner and Song (2002) was that this diagnostic growth rate appears to have a common threshold for all routes to breaking in deep water that we have examined, provides an earlier and more decisive indicator for the onset of breaking than previously proposed breaking thresholds, and may also provide an indicative measure of the strength of wave-breaking events. In subsequent sections of this paper, the distinctive behavior of the diagnostic parameters $\mu(t)$, $\langle\mu(t)\rangle$, and $\delta(t)$ are reported for the finite-water-depth environmental conditions under investigation.

3. Influence of mean water depth

To explore the influence of water depth on the diagnostic growth-rate parameter $\delta(t)$, an ensemble of cases of marginal recurrent and marginal breaking wave groups was investigated with the DAS code using the numerical channel shown in Fig. 1a with undisturbed water depth $h = 2$ and 4.

The evolution of a representative ensemble of marginally recurrent and marginal breaking wave groups was calculated for different initial group structures propagating over a flat bottom with different constant water depths. For each of these cases, the long-term evolution curves of $\langle\mu(t)\rangle$ and their corresponding growth-rate curves $\delta(t)$ have a similar behavior to the corresponding curves reported in SB02 for deep water evolution. Because of the pronounced crest–trough asymmetry of the nonlinear carrier waves at the envelope maximum, the diagnostic parameter $\mu(t)$ oscillates on a fast time scale, at about 2 times the carrier wave period for all cases. Its local average, $\langle\mu(t)\rangle$, increases continually for cases that proceed to breaking while for the recurrence cases, $\langle\mu(t)\rangle$ initially increases then ceases growing at the re-

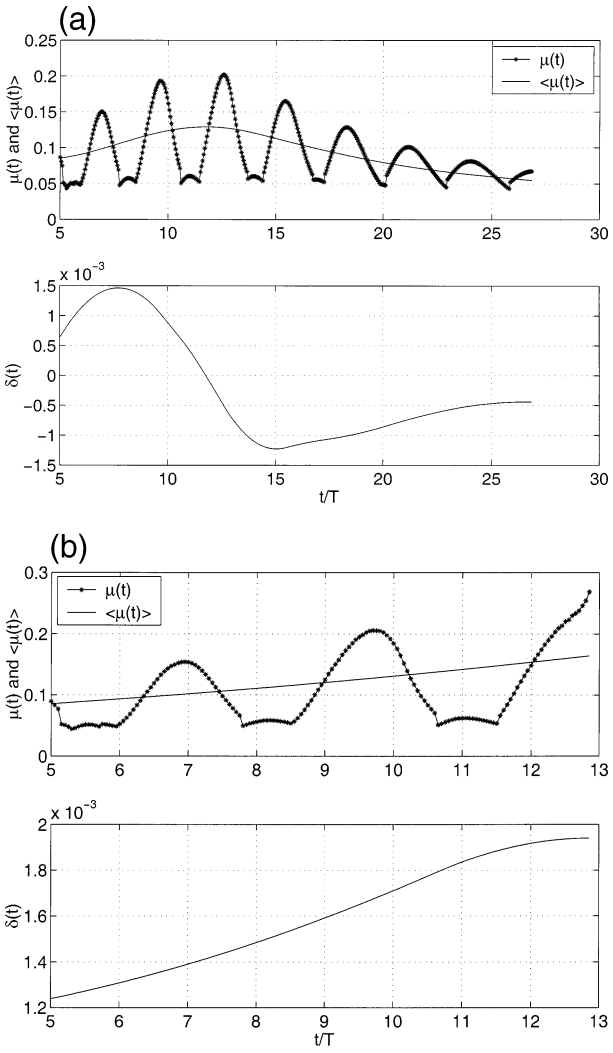

FIG. 2. (a) Long-term evolution of $\mu(t)$, $\langle\mu(t)\rangle$, and $\delta(t)$ for the marginal recurrence case III with $N = 5$, $A_p = 0.165$, and $h = 2$: (top) $\mu(t)$ and $\langle\mu(t)\rangle$, and (bottom) local average growth rate $\delta(t)$. (b) As in (a), but for the marginal breaking case III with $N = 5$, $A_p = 0.166$, and $h = 2$.

currence peak and then decreases as the recurrence cycle proceeds. The maximum growth rate $\delta^{\max}$ is seen to remain below the threshold level $\delta_{\text{th}} = 1.50 \times 10^{-3}$ for each recurrence case, while $\delta^{\max}$ exceeds this threshold value for all breaking cases. Thus the same threshold $\delta_{\text{th}} = 1.50 \times 10^{-3}$ found for deep water wave groups (SB02) is applicable for each of these illustrative cases of wave groups propagating in intermediate water depth over a flat bottom. The curves seen in Fig. 2 illustrate the typical long-term evolution behavior of $\mu(t)$, $\langle\mu(t)\rangle$, and $\delta(t)$ for marginally recurrent and marginal breaking wave groups with $N = 5$ traveling over a flat bottom with mean water depth $h = 2$.

Results for the full ensemble of cases investigated are summarized in Table 1 below, in which the symbols follow the notation used in SB02, and T is the carrier wave period, R denotes ''recurrence,'' and B indicates ''breaking.'' Of particular interest are the maximum diagnostic growth rate $\delta^{\max} = \max_t[\delta(t)]$ during the evolution, the breaking time t_{br}, the time t_{th} at which the growth rate $\delta(t)$ reaches the critical deep water breaking threshold value $\delta_{\text{th}} = 1.50 \times 10^{-3}$, the lead time to breaking $t_{\text{lead}} = t_{\text{br}} - t_{\text{th}}$, and the times $t_{\max}$ and t_{grmax} corresponding, respectively, to the times of the recurrence peak of $\mu(t)$ and the maximum growth rate of $\delta(t)$ for the recurrence cases. Related standard geometric and dynamical parameters of interest are also shown for comparison with previous results, for which all lengths are nondimensional quantities based on the carrier wavenumber $k_0 = 1$. Thus, $H_{\max}$ is the elevation of the maximum wave crest in the group above the mean trough level, that is, the height between the maximum crest and the mean level of the two adjacent troughs, $L_{\max}$ is the distance between the nearest two troughs associated with the maximum crest of the group at breaking or at the recurrence peak, and $U_r = H_{\max} L_{\max}^2/h^3$ is the Ursell number based on maximal wave parameters $H_{\max}$ and $L_{\max}$ at breaking or at the recurrence maximum. The Ursell number is a traditional parameter expressing the balance between shallow water wave steepening and the effect of the water acceleration (Peregrine 1983, p. 151), and when $U_r < 4\pi^2$, the effects of nonlinearity cannot be neglected. Table 1 indicates that all the cases reported here are in this category. Also, $(ak)_{\text{breaking}} = \pi H_{\max}/L_{\max}$ is the wave steepness at breaking onset and $H_{\max}/h$ is the breaker height index, the aspect ratio of breaking height:depth at the onset of breaking. The results for two marginally recurrent and breaking examples of case I wave groups investigated using the DP86 code for $N = 5$, $\lambda = 2\pi$, and $h = 2$ and 3 are also included in Table 1 for comparison.

From Table 1, it is seen that for each of the wave group structures studied, the piston movement parameter A_p, or equivalently the initial wave steepness s_0, for the marginal recurrence (R) cases increases systematically as the nondimensional water depth decreases. The same behavior is seen for the corresponding maximum value of wave steepness $(ak)_{\text{recur\_max}}$. The latter is consistent with the well-known result for steady unmodulated wave trains that nonlinear shallow water waves can have locally steeper surface profiles than their deep water counterparts (e.g., see Wiegel 1960, his Figs. 5, 6). This is often explained in terms of a modified balance between amplitude and frequency dispersion of the bound Fourier modes, allowing steeper nonbreaking carrier waves in shallower water than in deep water. Our findings, based on a limited number of realizations, suggest that a similar bottom influence can also occur for modulated wave packets, with these nonlinear wave profiles increasingly stabilized against breaking with decreasing mean water depth. Yet, despite this significant difference in surface profile geometry, the same breaking threshold growth rate of $\delta_{\text{th}} = 1.50 \times 10^{-3}$ found for deep water cases is seen to be applicable to the intermediate-depth ($h \geq 2$) wave groups

TABLE 1. Key results for wave groups traveling over a flat bottom for marginal recurrence and marginal breaking cases with different initial group structure, initial steepness s_0 or paddle amplitude A_p, undisturbed water depth h, and the number of waves N in the group: maximum wave height and wavelength parameters H_{max}, L_{max}, Ursell number U_r, local maximum steepness at recurrence $(ak)_{recur\_max}$ or breaking onset $(ak)_{breaking}$, breaker height index H_{max}/h, time when breaking threshold attained t_{th} or time of maximum recurrence growth rate t_{grmax}, time of breaking initiation t_{br} or recurrence maximum t_{max}, lead time for breaking $t_{lead} = t_{break} - t_{th}$, and diagnostic growth rate δ^{max}.

Cases	N	s_0	A_p	h	H_{max}	L_{max}	U_r	$(ak)_{breaking}$ or $(ak)_{recur\_max}$	H_{max}/h	t_{th} (or t_{grmax})	t_{br} (or t_{max})	t_{lead}	$\delta^{max} \times 10^3$
I (R)	5	0.122	—	3	0.551	5.367	0.5878	0.3225	0.1837	72.8T	88.7T	—	0.85
I (B)	5	0.123	—	3	0.618	5.572	0.7106	0.3484	0.2060	85.7T	86.8T	1.1T	2.84
I (R)	5	0.148	—	2	0.622	5.673	2.5022	0.3445	0.3110	88.4T	102.3T	—	0.76
I (B)	5	0.149	—	2	0.683	5.665	2.7399	0.3788	0.3415	87.8T	89.7T	1.9T	4.87
III (R)	5	—	0.127	4	0.671	6.754	0.4783	0.3121	0.1678	7.6T	15.4T	—	1.16
III (B)	5	—	0.128	4	0.704	6.754	0.5018	0.3275	0.1760	14.4T	15.5T	1.1T	1.68
III (R)	5	—	0.165	2	0.724	6.442	3.7557	0.3531	0.3620	7.7T	12.6T	—	1.46
III (B)	5	—	0.166	2	0.769	6.486	4.0438	0.3725	0.3845	8.2T	12.8T	4.6T	1.94
III (R)	8	—	0.110	4	0.738	7.289	0.6126	0.3181	0.1845	17.8T	21.9T	—	1.30
III (B)	8	—	0.111	4	0.782	7.289	0.6492	0.3370	0.1955	19.0T	22.0T	3.0T	1.64
III (R)	8	—	0.153	2	0.790	7.015	4.8595	0.3538	0.3950	15.8T	18.0T	—	1.36
III (B)	8	—	0.154	2	0.865	7.104	5.4567	0.3825	0.4325	15.7T	21.6T	5.9T	1.68
V (R)	5	—	0.065	2	0.512	4.812	1.4819	0.3343	0.2560	7.2T	12.5T	—	1.44
V (B)	5	—	0.066	2	0.562	4.857	1.6572	0.3635	0.2810	9.8T	12.6T	2.8T	2.47

investigated here. We note that this interesting result does not depend on the number of waves N in the group, just as was found in SB02 for deep water wave groups. Unfortunately, we were unable to examine even shallower conditions because the computed waveforms became ''ragged'' and we were reluctant to impose artificial numerical damping because it might have influenced the breaking onset process.

4. Influence of a bottom sandbar

To determine the effect of a localized bottom topographical feature on the onset of wave breaking in the present framework, we investigated an ensemble of wave groups with different initial group structures shoaling over the idealized ''sandbar'' located on an otherwise constant intermediate-depth environment. The typical computational domain is shown in Fig. 1b, and our study included a representative range of geometrical variations of the sandbar geometry and its location relative to the wave maker.

a. Long-term evolution

For comparison with water waves propagating over a flat bottom, Figs. 3 and 4 show two typical examples illustrating the influence of the bottom sandbar on the long-term evolution of $\mu(t)$, $\langle\mu(t)\rangle$, and $\delta(t)$ for the marginal recurrent and marginal breaking cases of the sandbar with different height h_0 located in a flat bottom $h = 4$.

We checked for visible impact of the bottom topography on the wave profiles, comparing representative wave surface profiles at their maximum recurrence configurations for an intermediate-depth case and two high-sandbar cases with the deep water cases studied in SB02. We estimated wave steepness as the product of the local wavenumber and one-half of the crest height above the mean trough level. The deep water waves had the lowest wave steepness level (0.3053), and the flat bottom topography with $h = 2$ had the highest (0.3546). The sandbar cases had maximum steepness levels of 0.3098 and 0.3197. However, this was not the most compelling difference. The surface profiles over sandbar topography appear to have higher, narrower crests and broader, flatter troughs and hence to be more nonlinear than the deep water case. Below, we investigate the influence of the increased nonlinearity for waves propagating in intermediate-depth water or experiencing the much shallower depth environment presented by the sandbar.

b. Diagnostic growth rates

Tables 2 and 3 summarize the key results obtained for a range of wave groups with different initial group structures shoaling over sandbars with different dimensions and different distances from the piston, calculated for water depths $h = 4$ and $h = 2$. Comparing the results in Tables 2 and 3 with Table 1, it is seen that the sandbar destabilizes the wave motion, consistent with the intuitive expectation that the sandbar induces an energy convergence that ''competes'' with the group-mediated convergence in the nonlinear wave packets. For example, we saw previously that marginally recurrent case III wave groups with $N = 5$ and $A_p = 0.127$ propagate over a flat bottom with $h = 4$. However, when a sandbar with height $h_0 = 2.0$ and length $l_0 = 30$ centered at $x_0 = 8\lambda$ ($\lambda = 2\pi$) is added, breaking occurs at $t = 15.6T$, with a corresponding maximum growth rate $\delta^{max} = 2.31 \times 10^{-3}$. For this same initial wave group geometry, when the height of the sandbar is increased to $h_0 = 2.5$ and the sandbar is lengthened to $l_0 = 8\lambda$, where $\lambda = 2\pi$, and centered farther downstream at $x_0 = 10\lambda$, breaking onset now occurs at $t = 15.5T$,

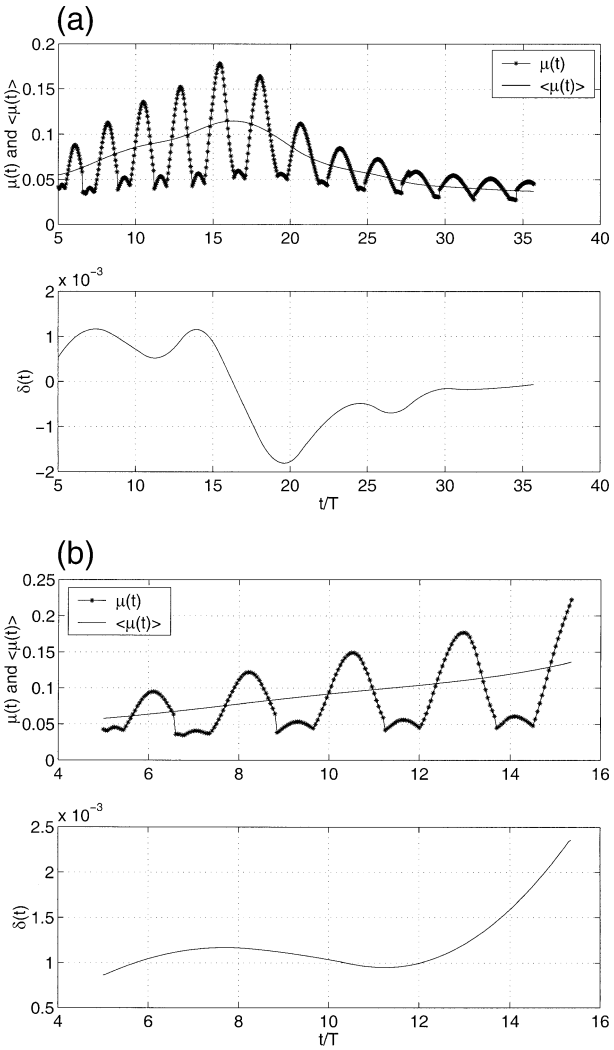

FIG. 3. (a) As in Fig. 2a, but for the marginal recurrence case III with $N = 5$, $A_p = 0.127$, $h = 4$, $l_0 = 8\lambda$, $x_0 = 10\lambda$, and $h_0 = 2.0$. (b) As in Fig. 2a, but for the marginal breaking case III with $N = 5$, $A_p = 0.128$, $h = 4$, $l_0 = 8\lambda$, $x_0 = 10\lambda$, and $h_0 = 2.0$.

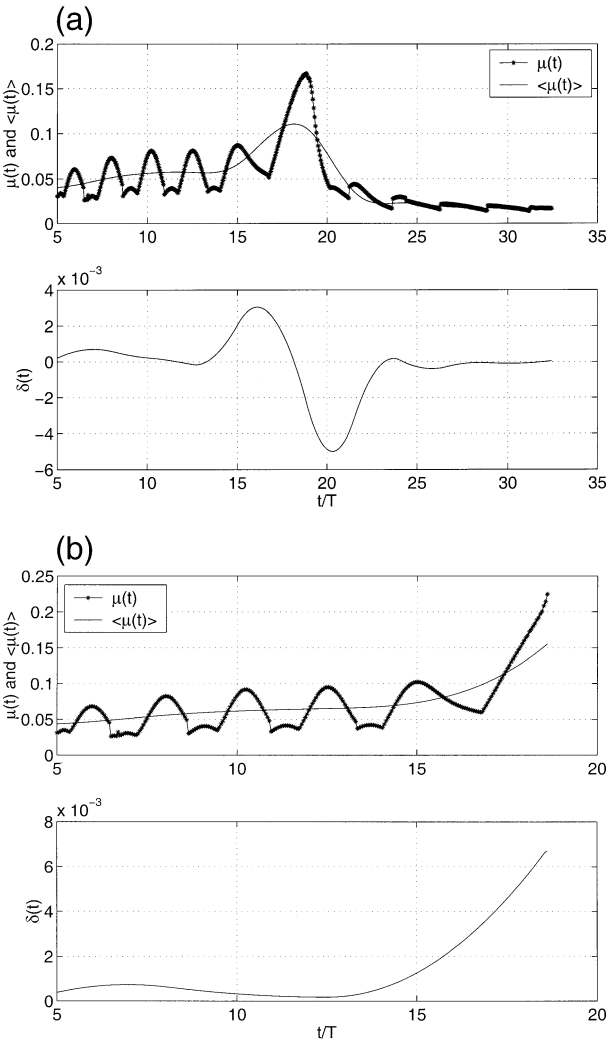

FIG. 4. (a) As in Fig. 2a, but for the marginal recurrence case III with $N = 5$, $A_p = 0.111$, $h = 4$, $l_0 = 8\lambda$, $x_0 = 10\lambda$, and $h_0 = 3.0$. (b) As in Fig. 2a, but for the marginal breaking case III with $N = 5$, $A_p = 0.112$, $h = 4$, $l_0 = 8\lambda$, $x_0 = 10\lambda$, and $h_0 = 3.0$.

with a much higher maximum growth rate $\delta^{\max} = 5.59 \times 10^{-3}$.

From Tables 2 and 3, it is seen also that the influence of the sandbar on the maximum growth rate $\delta^{\max}$ is negligible if the height of the sandbar h_0 is less than or equal to one-quarter of the still water depth h in which case the waves are only weakly modified by its presence—for example, sandbars with height $h_0 \leq 1$ in water depth $h = 4$ or $h_0 \leq 0.5$ for $h = 2$. Thus the proposed deep water breaking onset threshold level $\delta_{\text{th}} = 1.50 \times 10^{-3}$ is applicable for wave groups shoaling over a bottom sandbar if its height is sufficiently small. However, when the sandbar becomes high enough for the waves to strongly feel its presence, the maximum growth rate $\delta^{\max}$ for marginal recurrence, henceforth referred to as δ^R, now increases with the height of the bar. As shown in Tables 2 and 3, this occurs for sandbars with height $h_0 \geq 2.0$ in water depth $h = 4$ or $h_0 > 1.0$ for $h = 2$.

Further, for case III wave group traveling over a sandbar with $l_0 = 8\lambda$ and $x_0 = 10\lambda$, it is seen that δ^R increases from 1.17×10^{-3} to 3.05×10^{-3} when the height h_0 is increased from 2.0 to 3.0. Thus, the breaking threshold level δ_{th}, which lies between δ^R and the maximum growth rate for the marginal breaking case (henceforth referred to as δ^B) increases with the height of the sandbar. Moreover, it was found that the position of the bar has a significant influence on the evolution of wave groups and the breaking onset process, especially when the sandbar height exceeds one-quarter of the still water depth.

In summary, we tentatively attribute the effects described above to the increased nonlinearity, and hence stability in terms of amplitude dispersion, of the waves

TABLE 2. The H_{max}, L_{max}, δ_{max}, t_{th} (or t_{grmax}), t_{br} (or t_{max}), and t_{lead} for marginal recurrent and marginal breaking cases with $N = 5$ and $h = 4$ shoaling over a sandbar with different geometries and different distance from the piston. The symbols are described in the Table 1 caption.

Cases	A_p	l_0	h_0	x_0	H_{max}	L_{max}	t_{th} (or t_{grmax})	t_{br} (or t_{max})	t_{lead}	$\delta^{max} \times 10^3$
III (R)	0.127	30	1.0	8λ	0.679	6.666	11.6T	15.3T	—	1.20
III (B)	0.128	30	1.0	8λ	0.714	6.754	14.5T	15.5T	1.0T	1.68
III (R)	0.126	30	2.0	8λ	0.673	6.269	13.3T	15.5T	—	1.37
III (B)	0.127	30	2.0	8λ	0.707	6.313	13.4T	15.6T	2.2T	2.31
III (R)	0.103	30	3.0	8λ	0.553	6.140	13.6T	15.8T	—	3.11
III (B)	0.104	30	3.0	8λ	0.589	6.184	13.3T	15.9T	2.6T	6.33
III (R)	0.127	8λ	1.0	10λ	0.676	6.666	6.8T	15.4T	—	1.15
III (B)	0.128	8λ	1.0	10λ	0.714	6.666	14.9T	15.5T	0.6T	1.78
III (R)	0.127	8λ	2.0	10λ	0.688	6.489	14.0T	15.4T	—	1.17
III (B)	0.128	8λ	2.0	10λ	0.727	6.578	14.1T	15.4T	1.3T	2.36
III (R)	0.127	4λ	2.0	10λ	0.697	6.272	16.1T	17.9T	—	1.26
III (B)	0.128	4λ	2.0	10λ	0.710	6.622	15.2T	15.6T	0.4T	1.70
III (R)	0.127	2λ	2.0	10λ	0.677	6.754	14.0T	15.3T	—	1.21
III (B)	0.128	2λ	2.0	10λ	0.710	6.798	15.2T	15.3T	0.1T	1.58
III (B)	0.127	8λ	2.5	10λ	0.719	6.181	12.7T	15.5T	2.8T	5.59
III (R)	0.125	8λ	2.5	10λ	0.648	5.919	15.6T	18.4T	—	1.35
III (B)	0.126	8λ	2.5	10λ	0.742	6.008	14.5T	18.6T	4.1T	2.89
III (R)	0.111	8λ	3.0	10λ	0.579	5.965	16.1T	18.8T	—	3.05
III (B)	0.112	8λ	3.0	10λ	0.609	5.787	15.3T	18.6T	3.3T	6.71
III (R)	0.103	2λ	3.0	10λ	0.550	6.360	17.6T	19.7T	—	3.08
III (B)	0.104	2λ	3.0	10λ	0.580	6.406	17.9T	20.0T	2.1T	5.81

propagating in the shallower topography environment. Additional details of the dependence of the maximum growth rate δ^{max} on the variables h, h_0, l_0, and x_0 are discussed below.

c. Dependence of δ^{max} on the sandbar height

For wave groups that were recurrent when propagating over a flat bottom in ambient mean water depth h, breaking occurs when the height h_0 of the bar (width l_0, center x_0) is increased beyond a critical value. To illustrate this transition, Fig. 5 shows the average growth rate of $\langle \mu(t) \rangle$ for the same $N = 5$ wave group shoaling over a sandbar with different heights under conditions of fixed l_0 and x_0. The wave group was produced in ambient water depth $h = 4$ by the piston driven by the input (A2) with $A_p = 0.127$. The curves in Fig. 5 show the results for diagnostic growth rates for wave groups shoaling over our two standard sandbar geometries for different bar heights. These graphs show how the maximum growth rate δ^{max} increases as h_0 increases, with the onset of breaking for sufficiently high h_0, which is different for these two cases.

As noted above, for fixed l_0, x_0, and h, the maximum growth rate for marginal recurrence δ^R increases with h_0. In these two cases, the increase in δ^R is very modest for $h_0/h \leq 0.25$, and δ^R remains below the proposed deep water threshold $\delta_{th} = 1.50 \times 10^{-3}$. However, the breaking threshold was found to increase very significantly above this value when $h_0/h > 0.5$. For example, for case III wave groups shoaling over a sandbar with $l_0 = 8\lambda$, $x_0 = 10\lambda$ in mean water depth $h = 4$, δ^R increases to 3.05×10^{-3} when h_0/h is increased to 0.75.

d. Dependence of δ^{max} on the sandbar location

A sequence of numerical experiments revealed that the location x_0 of the sandbar also has a significant influence on the evolution of wave groups and the breaking process. Placing the sandbar in different positions modifies the evolution path of the wave groups and this can cause changes in the state of stability. For example, recurrent case III wave groups with $A_p = 0.112$, $N = 5$ and $h = 4$ shoaling over a sandbar with $l_0 = 8\lambda$ and $h_0 = 3.0$ develop into a breaking case if the same sandbar is shifted by 0.5 wavelength farther downstream, that is, from a center position of $x_0 = 9.5\lambda$ to $x_0 = 10\lambda$. Figure 6 shows more clearly the influence of the sand bar position on the evolution of the wave groups. These wave groups were produced by the piston motion (A2) with $A_p = 0.111$ in still water of depth $h = 4$.

In greater detail, we explored the marginal recurrence case of case III wave groups shoaling over a sandbar with $l_0 = 8\lambda$, $h_0 = 3.0$ and $h = 4$, for the range of sandbar center positions $x_0 = 9.5$, 9.75, 10, 10.25, and 10.5. The corresponding piston motion parameters A_p were 0.118, 0.111, 0.111, 0.112, and 0.114, and the associated maximum growth rates δ^R were respectively 3.07×10^{-3}, 3.31×10^{-3}, 3.05×10^{-3}, 2.62×10^{-3}, and 2.53×10^{-3}. The maximum growth rates δ^B of the corresponding marginal breaking cases (A_p was only increased by 0.001 in each case) were respectively 6.53×10^{-3}, 5.32×10^{-3}, 6.71×10^{-3}, 5.49×10^{-3}, and 4.24×10^{-3}. These results show that the magnitude of the growth rate δ^R (or δ^B) is sensitive to the center position x_0 of the sandbar. However, a breaking threshold can be found that is valid for all cases of sandbars with a fixed height, different widths, and located at dif-

TABLE 3. As for Table 2, but for marginal recurrent and marginal breaking cases with $N = 5$ and $h = 2$. The symbols are described in the Table 1 caption.

Cases	A_p	l_0	h_0	x_0	H_{max}	L_{max}	t_{th} (or t_{grmax})	t_{br} (or t_{max})	t_{lead}	$\delta^{max} \times 10^3$
III (R)	0.162	8λ	0.5	10λ	0.710	6.222	12.6T	16.1T	—	1.15
III (B)	0.163	8λ	0.5	10λ	0.748	6.355	9.9T	12.9T	3.0T	2.32
III (R)	0.153	8λ	0.8	10λ	0.650	6.047	13.3T	16.2T	—	1.97
III (B)	0.154	8λ	0.8	10λ	0.678	6.003	13.0T	16.1T	3.1T	4.88
III (R)	0.141	8λ	1.0	10λ	0.579	5.917	13.4T	16.3T	—	2.23
III (B)	0.142	8λ	1.0	10λ	0.631	6.005	13.2T	16.5T	3.3T	5.65
IV (R)	0.136	30	0.5	10λ	0.627	5.513	9.5T	18.8T	—	1.36
IV (B)	0.137	30	0.5	10λ	0.674	5.557	15.3T	19.1T	3.8T	1.84
IV (R)	0.131	30	0.8	10λ	0.597	5.382	16.4T	18.9T	—	2.15
IV (B)	0.132	30	0.8	10λ	0.647	5.470	15.4T	19.2T	3.8T	3.77
IV (R)	0.122	30	1.0	10λ	0.543	5.296	15.4T	18.7T	—	2.48
IV (B)	0.123	30	1.0	10λ	0.577	5.384	15.6T	19.0T	3.4T	5.72

ferent positions. For example, the threshold can be taken as 3.5×10^{-3} for the above examples of a bottom sandbar with $h_0 = 3.0$ in water depth $h = 4$. However, this threshold is more than 2 times the threshold found for the previous flat-bottom cases, and our results show that it increases systematically as the height of the bar is increased.

e. Dependence of δ^{max} on the sandbar width

For a sandbar with fixed h_0 and x_0 in still water depth h, increasing or decreasing the sandbar width l_0 causes the overall steepness of the bar to decrease or increase, respectively. Our calculations show that when h_0 is high enough to affect the breaking process, changing the sandbar length l_0 can cause a variation in the recurrence limit in relation to the required piston amplitude A_p. For example, as shown in Table 2, the marginal recurrence A_p decreases from 0.111 to 0.103 when l_0 decreases from 8λ to 2λ for case III wave groups with $h_0 = 3.0$, $x_0 = 10\lambda$ and $h = 4$, although the same marginal recurrence A_p is found when h_0 is taken as 2.0 and the other parameters remain the same. However, the influence of l_0 on δ^R is seen from Table 2 to be small and can be neglected, even for large h_0. For example, δ^R varies from 1.17×10^{-3} to 1.21×10^{-3} for the marginal recurrence cases ($h_0 = 2.0$, $x_0 = 10\lambda$ and $h = 4$) when l_0 is reduced from 8λ to 2λ. Even if h_0 is increased to 3.0, for the same change in l_0, δ^R only varies from 3.05×10^{-3} to 3.08×10^{-3}.

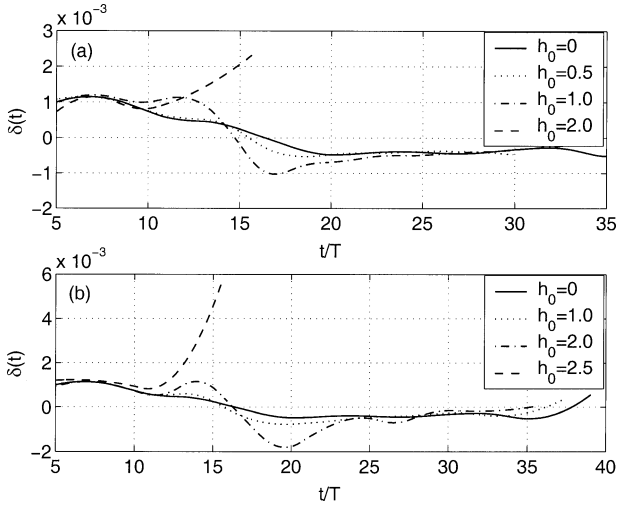

FIG. 5. The influence of sandbar height h_0 on the long-term evolution of $\delta(t)$ for case III with $\lambda = 2\pi$, $N = 5$, $A_p = 0.127$, and $h = 4$. (a) The sandbar has $l_0 = 30$, $x_0 = 8\lambda$, and $h_0 = 0$, 0.5, 1.0, and 2.0. (b) The sandbar has $l_0 = 8\lambda$, $x_0 = 10\lambda$, and $h_0 = 0$, 1.0, 2.0, and 2.5. The legend shows the symbols for the different sandbar heights.

f. Possible dependence of δ^{max} on sandbar steepness and height

In an effort to quantify the influence of the dimensions of the sandbar on the diagnostic growth rate parameter δ, we investigated the following two nondimensional aspect ratio parameters: (i) $2h_0/l_0$, a measure of the overall steepness of the sandbar, and (ii) h_0/h, the height of the bar at its center relative to the still water depth. The dependence of the critical maximum growth rate at recurrence on these two aspect ratios is shown in Fig. 7 for the cases investigated. It is seen that this growth rate depends in a complex way on these sandbar aspect ratios and their position. Therefore no simple relationship could be found between the breaking threshold level and the dimensionless quantities $2h_0/l_0$ and h_0/h.

5. Influence of water depth and a bottom sandbar on the breaking strength

We also investigated the influence of the still water depth and a bottom sandbar on the trend of the proposed breaking strength indicator δ^{max} with the overall packet steepness ak_c. As typical cases, we studied breaking case I wave groups with $N = 5$ and $\lambda = 2\pi$ traveling over a flat bottom of depth $h = 2$ and breaking case III wave groups with $N = 5$ and $\lambda = 2\pi$ traveling over a sandbar with height $h_0 = 3$, length $l_0 = 8\lambda$ and center at $x_0 = 10\lambda$ in still water depth $h = 4$.

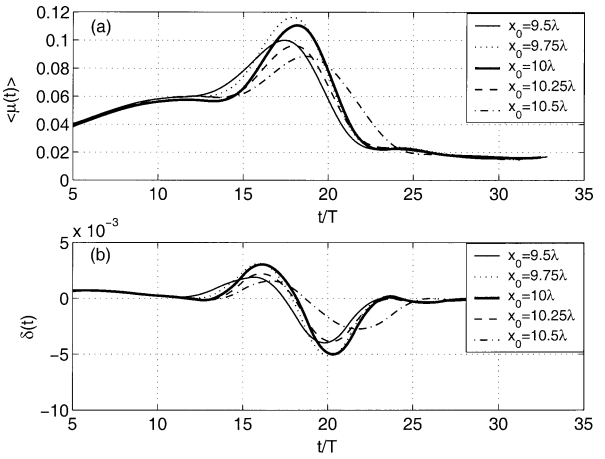

FIG. 6. The influence of sandbar location x_0 on the long-term evolution of $\langle \mu(t) \rangle$ and its growth rate $\delta(t)$ for case III with $N = 5$, $A_p = 0.111$, and $h = 4$ shoaling over a sandbar with $l_0 = 8\lambda$ and $h0 = 3.0$: (a) $\langle \mu(t) \rangle$ for $x_0 = 9.5\lambda$, 9.75λ, 10λ, 10.25λ, and 10.5λ and (b) the corresponding growth rates $\delta(t)$.

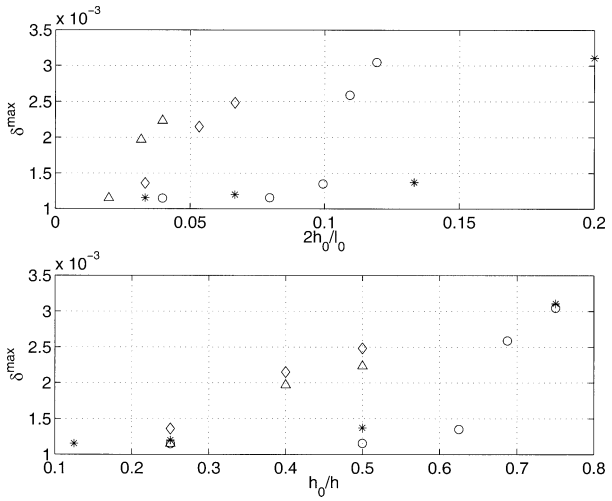

FIG. 7. The influence on the maximum growth rate $\delta^{\max}$ (i.e., δ^R) of (top) overall sandbar steepness $2h_0/l_0$ and (bottom) sandbar height-to-depth ratio h/h_0 for a range of marginal recurrence cases. Stars are for case III with $\lambda = 2\pi$, $N = 5$, and $h = 4$ shoaling over a bar with $l_0 = 30$ and $x_0 = 8\lambda$; open circles are for case III with $N = 5$ and $h = 4$ shoaling over a bar with $l_0 = 8\lambda$ and $x_0 = 10\lambda$; diamonds are for case IV with $N = 5$ and $h = 2$ shoaling over a bar with $l_0 = 30$ and $x_0 = 10\lambda$; triangles are for case III with $N = 5$ and $h = 2$ shoaling over a bar with $l_0 = 8\lambda$ and $x_0 = 10\lambda$.

For the case I breaking wave groups, the initial steepness parameters ak_c used were 0.1770, 0.1901, 0.2138, 0.2376, and 0.2613 (corresponding to initial carrier wave steepness input settings $s_0 = 0.149$, 0.160, 0.180, 0.200, and 0.222). As the wave packet steepness increased, the corresponding breaking times $t_{\rm br}/T$ were 89.7, 51.9, 34.6, 22.6, and 17.6, showing a rapid decrease. For the breaking case III wave groups, the ak_c investigated were 0.2591, 0.2658, 0.2769, 0.2881, and 0.2992 (corresponding to initial piston amplitudes $A_p = 0.112$, 0.115, 0.120, 0.125, and 0.130). The corresponding breaking times were found to be $t_{\rm br}/T = 18.6$, 18.3, 18.1, 15.7, and 13.1, with the associated horizontal breaking position $x_{\rm br}$ relative to the center x_0 of the sandbar given by $x_{\rm br}/x_0 = 1.01$, 0.98, 0.96, 0.85, and 0.67, respectively, confirming that initially steeper wave groups break progressively earlier and farther ''offshore.''

Of particular interest in this study is the corresponding trend of $\delta^{\max}$ with ak_c. These results are compared graphically in Fig. 8 with results for unforced deep water cases. In common with the deep water cases studied in SB02, $\delta^{\max}$ is found to increase with initial wave steepness while the corresponding breaking time $t_{\rm br}$ decreases. It is also noted, from the upper panel of Fig. 8, that the ambient water depths investigated only marginally influenced the maximum growth rate $\delta^{\max}$. However, the examples in the lower panel of Fig. 8 show that the sandbar can have a strong influence on $\delta^{\max}$ when the breaking takes place at the highest region of the bar. This can be seen in the lower panel of Fig. 8 for the breaking cases with smaller $ak_c = 0.2591$, 0.2658, and 0.2769, for which the relative breaking locations $x_{\rm br}/x_0$ are, respectively, 1.01, 0.98, and 0.96. However, for the steeper initial wave groups ($ak_c = 0.2881$ and 0.2992), the waves break well before they shoal over the bar (see previous paragraph) and, as shown in the lower panel of Fig. 8, the influence on $\delta^{\max}$ is negligible for such steeper wave groups.

As proposed in our previous papers (e.g., SB02), the behavior of the maximum growth-rate parameter $\delta^{\max}$ as the initial steepness is increased provides an encouraging qualitative correspondence with the breaking onset and strength observed by Rapp and Melville (1990). However, further research is needed to establish

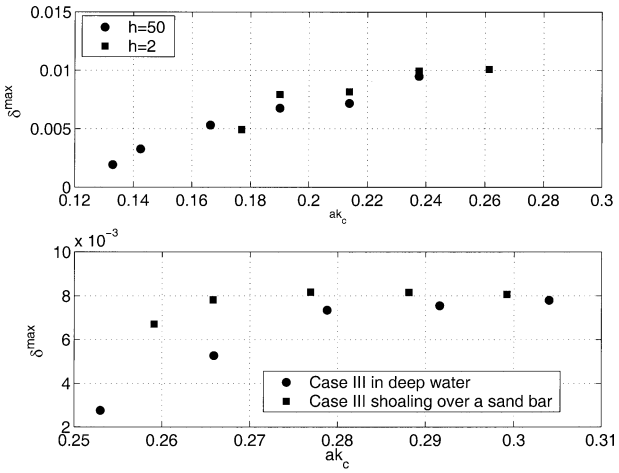

FIG. 8. The influence of ambient water depth or a bottom sandbar on the maximum growth rate $\delta^{\max}$ for breaking cases with different initial steepness ak_c. (top) Case I with $\lambda = 2\pi$ and $N = 5$ traveling over a flat bottom. (bottom) Case III with $\lambda = 2\pi$ and $N = 5$ shoaling over a sandbar with height $h_0 = 3.0$, length $l_0 = 8\lambda$, and center at $x_0 = 10\lambda$ in ambient water depth $h = 4$.

whether this proposed growth-rate parameter can reliably quantify the breaking strength. Confirmation of this proposition is beyond the scope of the present calculations because they do not address the postbreaking condition of the wave group and is left to future studies.

6. Conclusions

This computational study has investigated the onset of recurrence or breaking of two-dimensional wave groups in intermediate water depth or shoaling over a bottom sandbar. It used two fully nonlinear, two-dimensional inviscid free surface codes and a range of initial wave group geometries to investigate the behavior of a proposed diagnostic growth-rate parameter developed for deep water environments by Song and Banner (2002). Our results illustrate and quantify how the interaction of nonlinear wave groups with generic bottom topographic features influences the breaking onset process for shoaling waves. The main results are as follows.

1) Similar characteristics were found for the energy flux and energy focusing that occur within deep water wave groups for wave groups in finite constant water depth or in the presence of a sandbar. The onset of breaking is determined by a threshold in the maximum value $\delta^{\max}$ of the diagnostic growth-rate parameter.
2) For flat bottom topography, as the depth decreases, steeper (more nonlinear) waves can propagate without breaking in shallower water than in deep water, yet the same breaking threshold level $\delta_{\text{th}} = 1.50 \times 10^{-3}$ for the diagnostic growth rate is applicable both for deep and intermediate-depth water wave groups. This threshold is also valid for wave groups shoaling over a bottom sandbar provided that the height of the sandbar is less than or equal to one-quarter of the ambient water depth, in which case the influence of the sandbar is negligible.
3) Waves undergo significant and rapid steepening when they shoal over a sandbar if the height exceeds one-half of the ambient water depth. For this regime, we found that the threshold level of the diagnostic growth rate increases systematically with increasing height of the sandbar. This implies that the presence of sandbars can stabilize breaking onset, in the sense of increasing the energy convergence threshold growth rate for cases that would otherwise break in the absence of the sandbar influence. We attribute this tentatively to the increased nonlinearity of the waves and hence stability in terms of amplitude dispersion. In addition, the location of the sandbar with respect to the evolving wave group can have a significant influence on the breaking-onset process, especially when the height of the bar is substantial.
4) Following Song and Banner (2002), the present results suggest that the strength of breaking events may be related to the mean rate of convergence of energy at the group maximum immediately preceding breaking onset and is reflected by the corresponding value of the diagnostic growth rate $\delta(t_{\text{br}})$ just prior to breaking. For the cases we investigated with $k_0 h > 2$, we found only a marginal influence on the growth rate $\delta(t_{\text{br}})$ for wave groups in intermediate water depth with a flat bottom. However, a bottom sandbar has a stronger influence on $\delta(t_{\text{br}})$ when its height exceeds one-half of the still water depth and breaking takes place at the highest region of the bar, suggesting that much stronger breaking will ensue.

Acknowledgments. The authors gratefully acknowledge the financial support of the Australian Research Council for this project. Author J. B. Song also gratefully acknowledges the support of the 100-Talent Project of the Chinese Academy of Sciences (No. 524) and the National Natural Science Foundation of China (No. 40376008).

APPENDIX

Details of Wave Groups Investigated

Case I comprised a fundamental carrier wave with two small symmetric sidebands, using as parameters the initial carrier wave amplitude a_0 (or steepness $s_0 = a_0 k_0$, where $k_0 = 1$) and the number of waves in one modulation length, N. The initial wave group had the structure of a uniform, steady, finite-amplitude wave train whose linear approximation is $\eta = a_0 \cos(k_0 x)$, where $k_0 = 1$. On this primary wave are superimposed perturbations having the initial form

$$\varepsilon a_0 \cos\left(\frac{N+1}{N} k_0 x - \theta\right) + \varepsilon a_0 \cos\left(\frac{N-1}{N} k_0 x - \theta\right), \quad \text{with } \varepsilon = 0.1 \quad \text{and} \quad k_0 = 1. \tag{A1}$$

Here, N is the integer number of waves in the group, where $3 \le N \le 10$. This is the range used by DP86 and provides sideband perturbation wavenumbers in the range [0.667, 1.333]. Also, following DP86, the phase angle θ was taken as $\pi/4$ because it provides the most rapid initial growth of the sideband modes.

Case III was generated using the DAS code by a piston wave maker driven by the motion

$$x_p = -0.25 A_p \left(\tanh\frac{4\omega t}{N\pi} + 1\right)\left[1 - \tanh\frac{4(\omega t - 2N\pi)}{N\pi}\right] \times \sin\left[\omega\left(t - \frac{0.018 t^2}{2}\right)\right], \tag{A2}$$

where, as in SB02, t is time, N is an integer that controls the number of waves produced by the piston, A_p is proportional to the piston amplitude, $\omega = \sqrt{g(2\pi/\lambda)\tanh(2\pi h/\lambda)}$ is its angular frequency, λ is the carrier wavelength, and h is the still water depth. For comparison, we also investigated two other wave group geometries designated, respectively, cases IV and V. Case IV wave groups were generated by the piston wave maker driven by the motion

$$x_p = \begin{cases} -A_p\left[\sin(\omega t) - 0.1\sin\left(\dfrac{N+1}{N}\omega t - \dfrac{\pi}{4}\right) - 0.1\sin\left(\dfrac{N-1}{N}\omega t - \dfrac{\pi}{4}\right)\right] & (0 \le \omega t \le 2N\pi) \\ 0 & \text{(all other times).} \end{cases} \tag{A3}$$

Case V, with a much more rapid deformation than case III and case IV, was produced by the piston displacement given by

$$x_p = \begin{cases} -A_p\left[\cos\left(\omega t - \dfrac{19N\pi}{18}\right) - \cos\left(\dfrac{N+1}{N}\omega t - \dfrac{19N\pi}{18}\right)\right] & (0 \le \omega t < 2N\pi) \\ 0 & \text{(all other times).} \end{cases} \tag{A4}$$

To simulate intermediate-depth water waves, the undisturbed water depth near the piston was taken as $h = 2$ or 4.

REFERENCES

Banner, M. L., and D. H. Peregrine, 1993: Wave breaking in deep water. *Annu. Rev. Fluid Mech.,* **25,** 373–397.

——, and J.-B. Song, 2002: On determining the onset and strength of breaking for deep water waves. Part II: Influence of wind forcing and surface shear. *J. Phys. Oceanogr.*, **32,** 2559–2570.

——, J. R. Gemmrich, and D. M. Farmer, 2002: Multiscale measurements of ocean wave breaking probability. *J. Phys. Oceanogr.,* **32,** 3364–3375.

Beji, S., and J. A. Battjes, 1993: Experimental investigation of wave-propagation over a bar. *Coastal Eng.,* **19,** 151–162.

Dold, J. W., and D. H. Peregrine, 1986: Water-wave modulation. *Proc. 20th Int. Conf. on Coastal Engineering,* Tapei, Taiwan, ASCE, 163–175.

Duncan, J. H., 2001: Spilling breakers. *Annu. Rev. Fluid Mech.,* **33,** 519–547.

Elgar, S., R. T. Guza, B. Raubenheimer, T. H. C. Herbers, and E. L. Gallagher, 1997: Spectral evolution of shoaling and breaking waves on a barred beach. *J. Geophys. Res.,* **102,** 15 797–15 805.

Kuriyama, Y., 2002: Medium-term bar behavior and associated sediment transport at Hasaki, Japan. *J. Geophys. Res.,* **107,** 3132, doi:10.1029/2001JC000899.

Lippmann, T. C., R. A. Holman, and K. K. Hathaway, 1993: Episodic, nonstationary behavior of a double bar system at Duck, North Carolina, U.S.A. 1986–1991. *J. Coastal Res.,* **15,** 49–75.

Melville, W. K., 1996: Wave breaking in air–sea interaction. *Annu. Rev. Fluid Mech.,* **28,** 279–321.

——, and P. Matusov, 2002: Distribution of breaking waves at the ocean surface. *Nature,* **417,** 58–63.

Nelson, R. C., 1994: Depth limited design wave heights in very flat regions. *Coastal Eng.,* **23,** 43–59.

Peregrine, D. H., 1983: Breaking waves on beaches. *Annu. Rev. Fluid Mech.,* **15,** 149–178.

Plant, N. G., R. A. Holman, M. H. Freilich, and W. A. Birkemeier, 1999: A simple model for interannual sandbar behavior. *J. Geophys. Res.,* **104,** 15 755–15 776.

Rapp, R. J., and W. K. Melville, 1990: Laboratory measurements of deep water breaking waves. *Philos. Trans. Roy. Soc. London,* **A331,** 735–800.

Ruessink, B. G., and A. Kroon, 1994: The behavior of a multiple bar system in the nearshore zone of Terscheling, the Netherlands: 1965–1993. *Mar. Geol.,* **121,** 187–197.

Shand, R. D., and D. G. Bailey, 1999: A review of net offshore bar migration with photographic illustrations from Wanganui, New Zealand. *J. Coastal Res.,* **15,** 365–378.

Song, J.-B., and M. L. Banner, 2002: On determining the onset and strength of breaking for deep water waves. Part I: Unforced irrotational wave groups. *J. Phys. Oceanogr.,* **32,** 2541–2558.

Svendsen, I. A., and J. Veeramony, 2001: Wave breaking in wave groups. *Waterw. Port Coastal Ocean Div.,* **127,** 200–212.

Thorpe, S. A., 1995: Dynamical process of transfer at the sea surface. *Progress in Oceanography,* Vol. 35, Pergamon, 315–352.

Tulin, M. P., and T. Waseda, 1999: Laboratory observations of wave group evolution, including breaking effects. *J. Fluid Mech.,* **378,** 197–232.

Wiegel, R. L., 1960: A presentation of cnoidal wave theory for practical application. *J. Fluid Mech.,* **7,** 273–286.

Wijnberg, K. M., and J. H. J. Terwindt, 1995: Extracting decadal morphological behaviour from high-resolution, long-term bathymetric surveys along the Holland coast using eigenfunction analysis. *Mar. Geol.,* **126,** 301–336.